Electronic Supplementary Information

Surface overgrowth on gold nanoparticles modulating high-energy facets for efficient electrochemical CO_2 reduction

Woong Choi,[a,‡,§] *Joon Woo Park,*[a,§] *Woonghyeon Park,*[b]
*Yousung Jung,**[,b] *and Hyunjoon Song**[,a]

a. Department of Chemistry, Korea Advanced Institute of Science and Technology (KAIST), Daejeon 34141, Republic of Korea. E-mail: hsong@kaist.ac.kr

b. Department of Chemical and Biomolecular Engineering (BK21 four), Korea Advanced Institute of Science and Technology (KAIST), Daejeon 34141, Republic of Korea. E-mail: ysjn@kaist.ac.kr

‡ Present Address: Clean Energy Research Center, Korea Institute of Science and Technology (KIST), Seoul 02792, Republic of Korea.

§ These authors contributed equally.

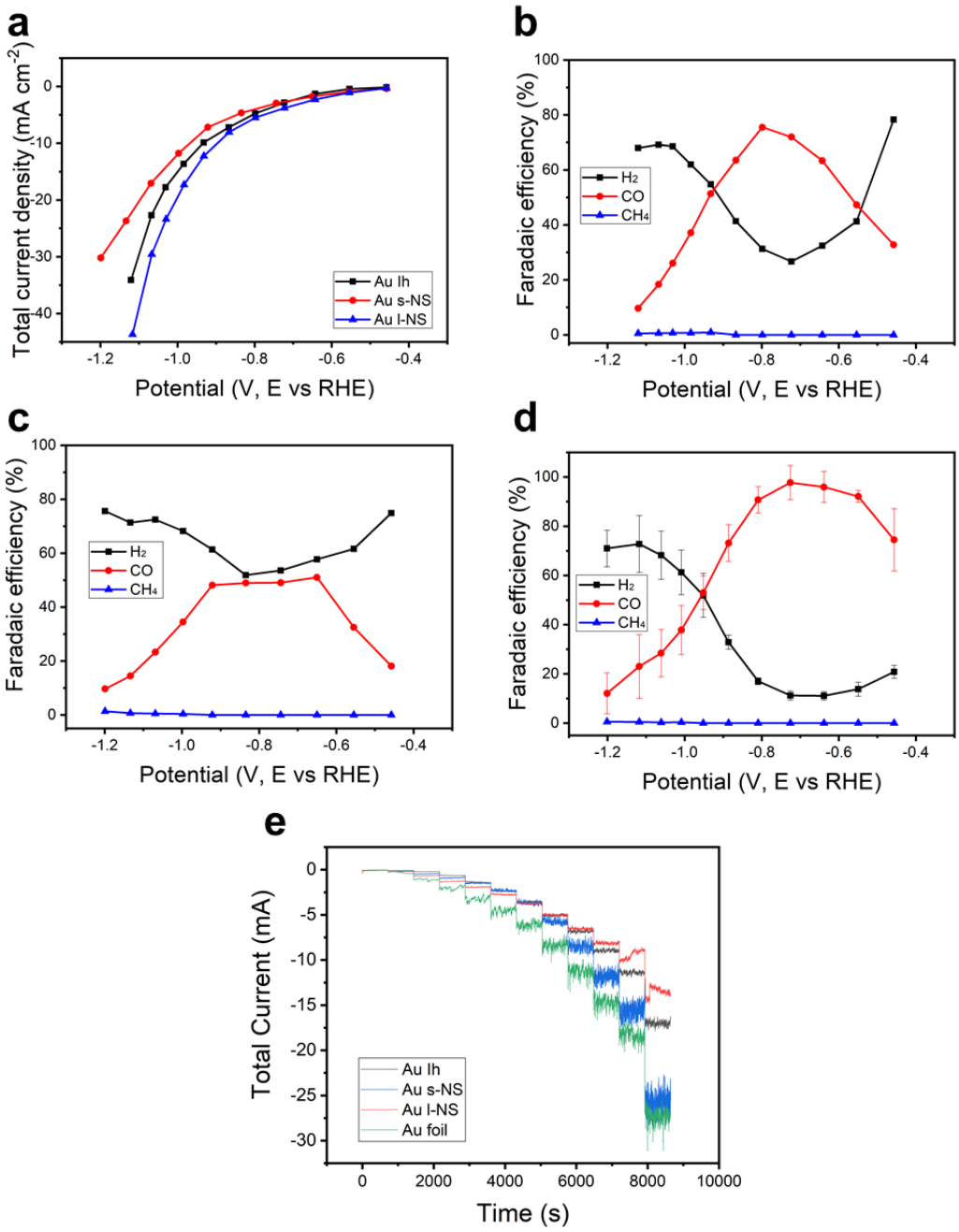

Fig. S1 (a) Total current densities and partial Faradaic efficiencies of the gaseous products during eCO_2RR using (b) **Ih**, (c) **s-NS,** and (d) **l-NS**. (e) i-t graph of potential-dependent eCO_2RR measurements of **Ih**, **s-NS**, **l-NS,** and Au foil.

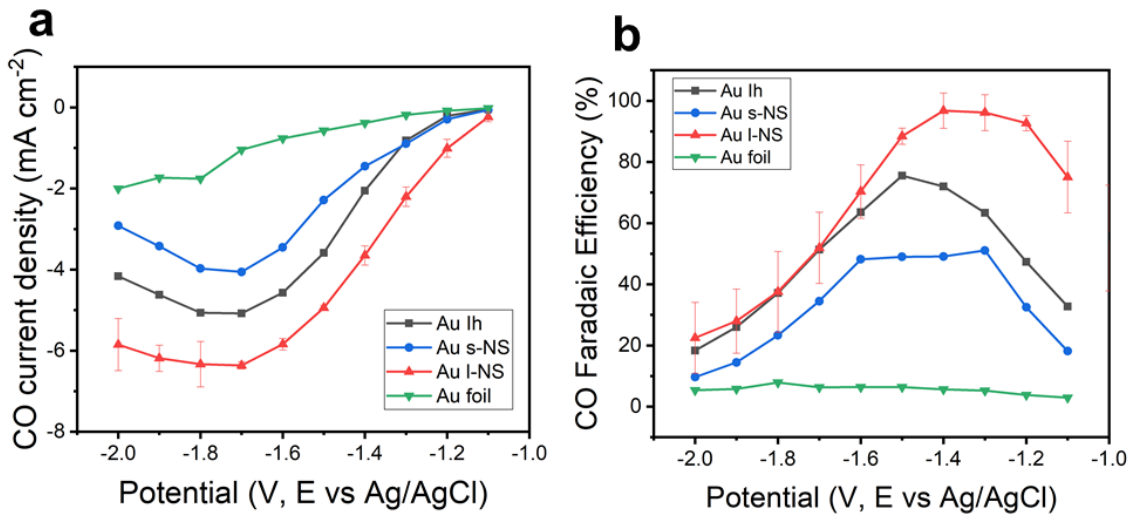

Fig. S2 (a) CO current densities and (b) Faradaic efficiencies of Au catalysts with applied potentials vs. Ag/AgCl without iR correction.

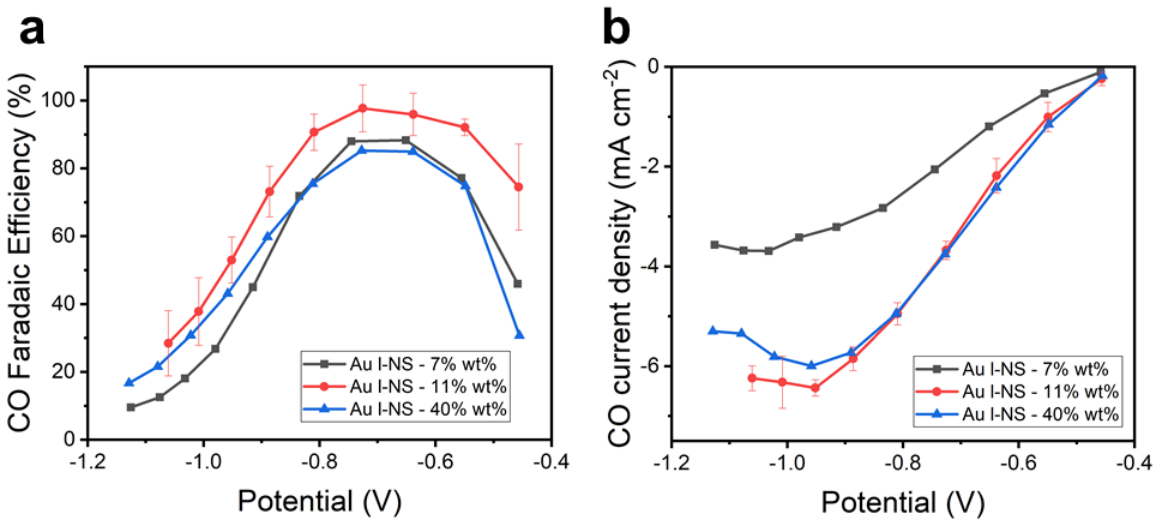

Fig. S3 (a) CO current densities and (b) Faradaic efficiencies of Au/C catalysts with Au loading ratios of 7, 11, and 40 wt %.

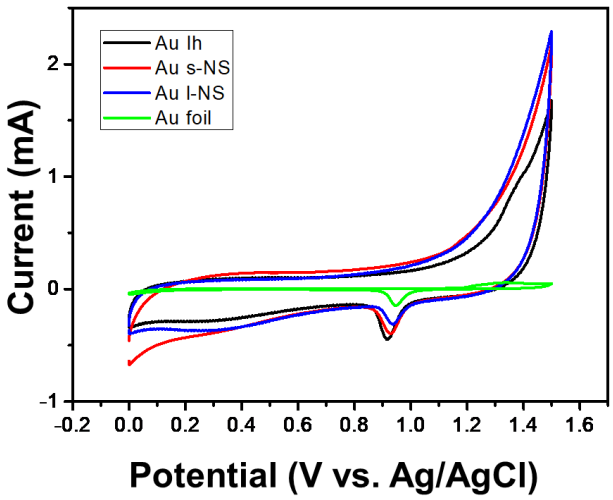

Fig. S4 Cyclic voltammograms (CV) for ECSA measurements of the Au catalysts. The CVs were performed in a 50 mM H_2SO_4 electrolyte at a scan rate of 50 mV s^{-1}.

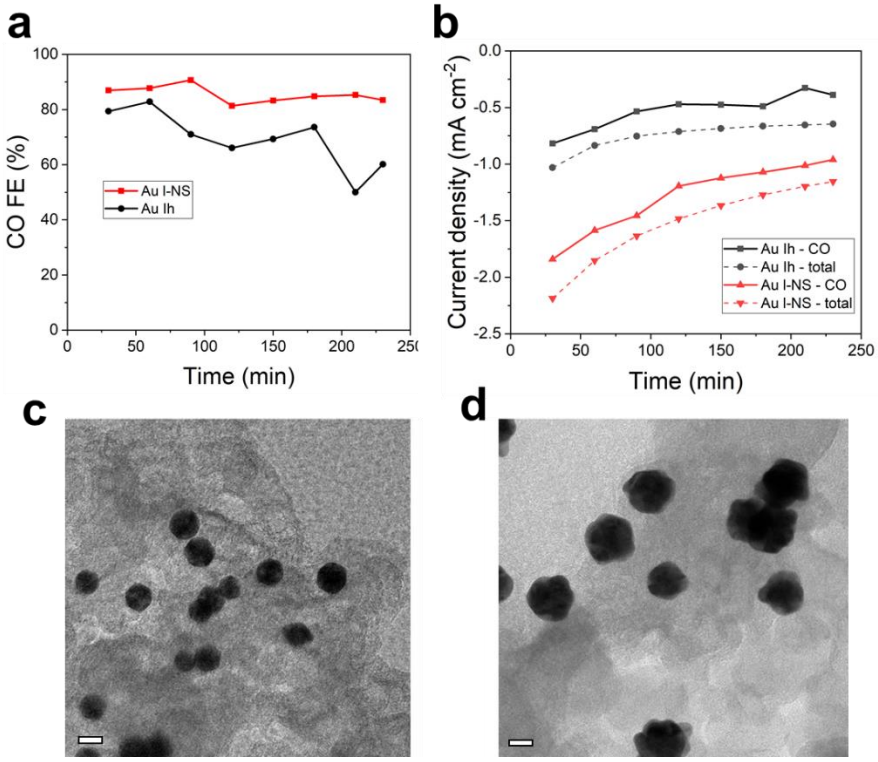

Fig. S5 (a) The CO FEs and (b) current densities of **Ih** (black) and **l-NS** (red) during the durability test for 4 h. TEM images of (c) **Ih** and (d) **l-NS** on the conductive carbon materials after the durability test. The bars represent 20 nm.

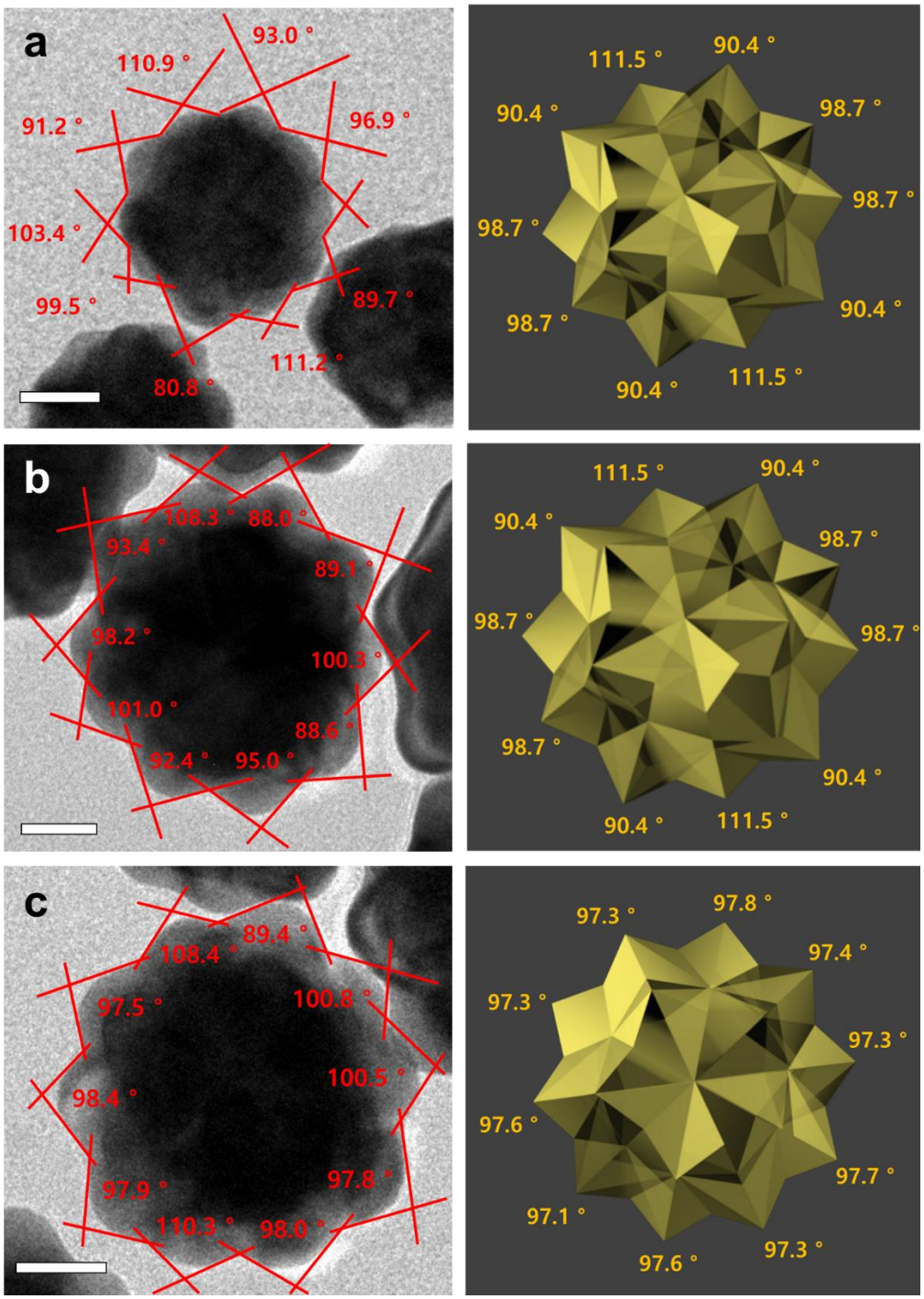

Fig. S6 Additional TEM images of **l-NS** and their corresponding projections of the three-dimensional model covered solely with {321} facets on the surface. The average angle deviations are (a) 2.3, (b) 4.3, and (c) 4.1 degrees. The bars represent 20 nm.

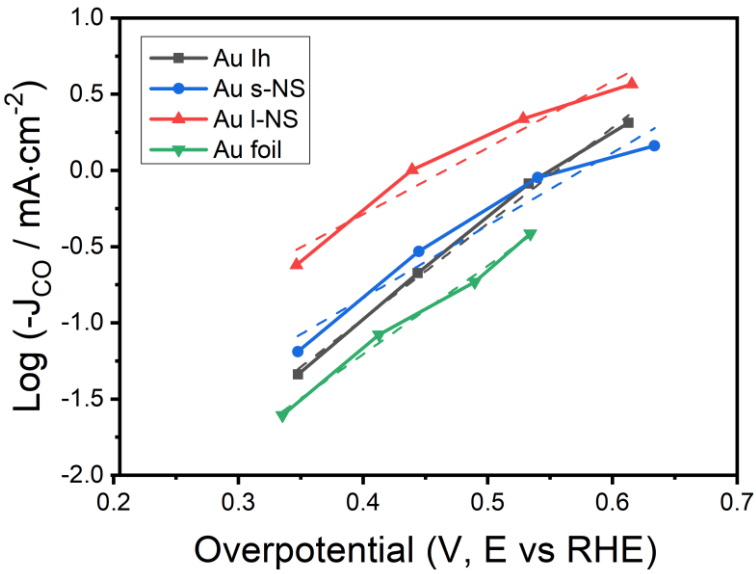

Fig. S7 Tafel plots of CO production on **Ih** (black), **s-NS** (blue), **l-NS** (red), and Au foil (green). Solid lines represent experimental values, and dash lines represent trend lines for measuring the Tafel slopes.

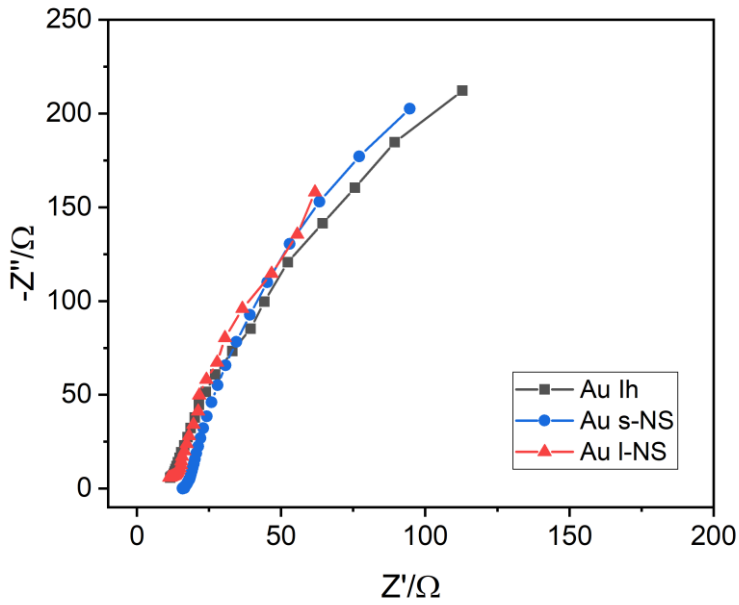

Fig. S8 Nyquist plots of **Ih** (black), **s-NS** (blue), and **l-NS** (red) from EIS at -0.36 V vs. RHE.

Table S1. Faradaic efficiencies and mass activities of Au and Ag nanocatalysts for eCO_2RR.

Catalysts	E vs RHE (V)	CO FE (%)	CO Mass Activity ($A\ g^{-1}$)	Electrolyte	Membrane	Ref.
This Work	**-0.7**	**95**	**121.6**	**0.5 M $KHCO_3$**	**Nafion**	
Au NPs	-0.52	97	3	0.5 M $KHCO_3$	Nafion	1
Au NPs	-1.2	45	-	0.1 M $KHCO_3$	-	2
Au rhombohedral	-1.0	70	9	0.5 M $KHCO_3$	without membrane	3
Au nanowires	-0.35	94	1.84	0.5 M $KHCO_3$	Nafion	4
Ag NPs with cysteine	-0.75	84.4	30	0.5 M $KHCO_3$	Nafion	5
Oleylamine capped Ag NPs	-0.75	92.6	75	0.5 M $KHCO_3$	Nafion	6
Ag triangle NPs	-0.855	96.8	-	0.1 M $KHCO_3$	Nafion	7
Ag@Au core-shell nanowires	-1.2	99.3	11.8	0.1 M KCl	Nafion	8
Au NPs on mesoporous carbon	-0.66	80	12	0.5 M $KHCO_3$	No membrane (glass frit)	9
$Au_{80}Ag_{20}$ NPs, ~25 nm	-0.7	60	3.7	0.1 M $NaHCO_3$	Nafion	10
Au_{25} cluster/C	-1.0	Appox. 100	-	0.1 M $KHCO_3$	Nafion	11
$Au_{44}(TBBT)_{28}$ cluster/C	-0.57	83	30.8	0.5 M $KHCO_3$	Nafion	12

Table S1. (cont.).

Catalysts	E vs RHE (V)	CO FE (%)	CO Mass Activity ($A\ g^{-1}$)	Electrolyte	Membrane	Ref.
$Au_{47}Cd_2(TBBT)_{31}$ cluster/C	-0.57	96	55.6	0.5 M $KHCO_3$	Nafion	12
Amidinate-protected Au_{28} cluster/CNT	-0.57	96.5	79.0 (-0.6 V) 113.0 (-0.7 V) 318.7 (-0.87 V)	0.5 M $KHCO_3$	Nafion	13
Oleylamine-capped Au NP	-0.65	63.5	23.2 (-0.65 V) 35.8 (-0.7 V) (approx.)	0.5 M $KHCO_3$	Selemion	14
Porphyrin-modified Au NP	-0.45	94	221 (-0.65 V) 262 (-0.7 V) (approx.)	0.5 M $KHCO_3$	Selemion	14
PEG-modified commercial Au/C	-0.77	75.6	-	0.5 M $KHCO_3$	N/A	15
PEG-modified liquid-medium sputtering Au/C	-0.57	100	-	0.5 M $KHCO_3$	N/A	15
Au-N-heterocyclic carbene NP	-0.57	83%	-	0.1 M $KHCO_3$	Selemion AMV	16

Table S2. Integration values of Au catalysts from CVs for calculating ECSAs.

Catalysts	Ih	s-NS	l-NS	Au foil
Integration value (A·V)	2.37×10^{-5}	1.96×10^{-5}	1.17×10^{-5}	8.53×10^{-6}
ECSA (cm^2)	1.06	0.88	0.52	0.38

Supplementary Methods

Calculation of Faradaic Efficiency

The equation below shows how the Faradaic efficiency ($\mathbf{FE_{gas}}$) for each gaseous product was derived.

$$\boldsymbol{FE_{gas}} = \frac{\boldsymbol{i_{gas}}}{\boldsymbol{i_{total}}} \times \mathbf{100}\ \left(\boldsymbol{where,\ i_{gas}} = \boldsymbol{c_{gas}} \times \boldsymbol{f} \times \frac{\boldsymbol{n_{gas} F p_0}}{\boldsymbol{RT}}\right)$$

The current density of the products ($\mathbf{i_{gas}}$) was derived from the concentrations ($\mathbf{c_{gas}}$) measured by integrating the peaks of gas chromatogram results. $\mathbf{n_{gas}}$ is 2 for both H_2 and CO. **f**, **F**, $\mathbf{p_0}$, **R**, and **T** stands for flow rate, faradaic constant, gas pressure, ideal gas constant, and temperature, respectively.[17]

Calculation of ECSA values

The peak from the oxidation scan at 0.9 to 1.0 V vs. Ag/AgCl was integrated, where the integration value is proportional to ECSA, scan rate, and reduction charge per unit area.

$$ECSA(cm^{-2}) = \frac{Intergration\ value(A \cdot V)}{scan\ rate(V \cdot s^{-1}) \times reduction\ charge\ per\ unit\ area\ (C \cdot cm^{-2})}$$

Generalized coordination number (GCN)

The GCN of atom i is estimated as follows:

$$GCN(i) = \sum_{j=1}^{n_i} \frac{cn(j) n_j}{cn_{max}}$$

where cn(j) is a usual coordination number of neighboring atoms of i and cn_{max} is the maximum number of the first-nearest neighbors in bulk.[18]

References

1. W. Zhu, R. Michalsky, Ö. Metin, H. Lv, S. Guo, C. J. Wright, X. Sun, A. A. Peterson and S. Sun, *J. Am. Chem. Soc.*, 2013, **135**, 16833-16836.

2. H. Mistry, R. Reske, Z. Zeng, Z.-J. Zhao, J. Greeley, P. Strasser and B. R. Cuenya, *J. Am. Chem. Soc.*, 2014, **136**, 16473-16476.

3. H.-E. Lee, K. D. Yang, S. M. Yoon, H.-Y. Ahn, Y. Y. Lee, H. Chang, D. H. Jeong, Y.-S. Lee, M. Y. Kim and K. T. Nam, *ACS Nano*, 2015, **9**, 8384-8393.

4. W. Zhu, Y.-J. Zhang, H. Zhang, H. Lv, Q. Li, R. Michalsky, A. A. Peterson and S. Sun, *J. Am. Chem. Soc.*, 2014, **136**, 16132-16135.

5. C. Kim, H. S. Jeon, T. Eom, M. S. Jee, H. Kim, C. M. Friend, B. K. Min and Y. J. Hwang, *J. Am. Chem. Soc.*, 2015, **137**, 13844-13850.

6. C. Kim, T. Eom, M. S. Jee, H. Jung, H. Kim, B. K. Min and Y. J. Hwang, *ACS Catal.*, 2017, **7**, 779-785.

7. S. Liu, H. Tao, L. Zeng, Q. Liu, Z. Xu, Q. Liu and J.-L. Luo, *J. Am. Chem. Soc.*, 2017, **139**, 2160-2163.

8. J. Liu, Y. Wang, H. Jiang, H. Jiang, X. Zhou, Y. Li and C. Li, *Chem. Asian J.*, 2020, **15**, 425-431.

9. M. Miola, X.-M. Hu, R. Brandiele, E. T. Bjerglund, D. K. Grønseth, C. Durante, S. U. Pedersen, N. Lock, T. Skrydstrup and K. Daasbjerg, *J. CO_2 Util.*, 2018, **28**, 50-58.

10. A. M. Ismail, E. Csapó and C. Janáky, *Electrochim. Acta*, 2019, **313**, 171-178.

11. D. R. Kauffman, D. Alfonso, C. Matranga, H. Qian and R. Jin, *J. Am. Chem. Soc.*, 2012, **134**, 10237-10243.

12. S. Zhuang, D. Chen, L. Liao, Y. Zhao, N. Xia, W. Zhang, C. Wang, J. Yang and Z. Wu, *Angew. Chem. Int. Ed.*, 2020, **59**, 3073-3077.

13. S.-F. Yuan, R.-L. He, X.-S. Han, J.-Q. Wang, Z.-J. Guan and Q.-M. Wang, *Angew. Chem. Int. Ed.*, 2021, **60**, 14345-14349.

14. Z. Cao, S. B. Zacate, X. Sun, J. Liu, E. M. Hale, W. P. Carson, S. B. Tyndall, J. Xu, X. Liu, X. Liu, C. Song, J.-h. Luo, M.-J. Cheng, X. Wen and W. Liu, *Angew. Chem. Int. Ed.*, 2018, **57**, 12675-12679.

15. M. W. Chung, I. Y. Cha, M. G. Ha, Y. Na, J. Hwang, H. C. Ham, H.-J. Kim, D. Henkensmeier, S. J. Yoo, J. Y. Kim, S. Y. Lee, H. S. Park and J. H. Jang, *Appl. Catal., B*, 2018, **237**, 673-680.

16. Z. Cao, D. Kim, D. Hong, Y. Yu, J. Xu, S. Lin, X. Wen, E. M. Nichols, K. Jeong, J. A. Reimer, P. Yang and C. J. Chang, *J. Am. Chem. Soc.*, 2016, **138**, 8120-8125.

17. J. Kim, W. Choi, J. W. Park, C. Kim, M. Kim and H. Song, *J. Am. Chem. Soc.*, 2019, **141**, 6986-6994.

18. F. Calle-Vallejo, J. I. Martínez, J. M. García-Lastra, P. Sautet and D. Loffreda, *Angew. Chem. Int. Ed.*, 2014, **53**, 8316-8319.